Sensors and Materials, Vol. 27, No. 8 (2015) 743–754
MYU Tokyo

S & M 1111

A Novel Reliable and Low-Cost Wireless Thermal Convection-Type Angular Accelerometer Made Directly on a Flexible Substrate

Jium-Ming Lin*, Cheng-Hung Lin[1] and Chia-Hsien Lin[2]

Department of Electronic Engineering, Chung-Hua University,
707, Sec. 2, Wu-Fu Rd., Hsin-chu, 30012, Taiwan
[1]Ph.D. Program in Engineering Science, College of Engineering, Chung-Hua University,
707, Sec. 2, Wu-Fu Rd., Hsin-chu, 30012, Taiwan
[2]Graduate Institute of Electrical Engineering, Chung-Hua University,
707, Sec. 2, Wu-Fu Rd., Hsin-chu, 30012, Taiwan

(Received July 2, 2014; accepted May 11, 2015)

Key words: radio frequency identification (RFID)-based angular accelerometer, nonfloating type, thermal convection, thermal sensors

Five novel ideas are proposed for integrating an active radio frequency identification (RFID) tag with a thermal convection angular accelerometer on a flexible substrate. The first two ideas are to fabricate the device directly on a flexible substrate (*e.g.*, polyimide) and without any movable parts. The flexible substrate thermal conductivity is much lower than that of silicon, so the new substrate can save more power and be very reliable. The third idea is to apply xenon gas in the chamber for heat convection instead of the traditional carbon dioxide, so that the heater and thermal sensors have no oxidation and performance degradation effects. The fourth idea is to integrate the angular accelerometer with an active RFID tag on the same substrate; thus, the device becomes a more useful wireless sensor. The final idea is to apply a hemispherical chamber instead of the conventional rectangular one to increase the sensitivity and response speed of the angular accelerometer. Although both sensitivity and response speed are lower than those of the floating one, the nonfloating device may be a choice if reliability and cost are the major concerns. Moreover, for the angular acceleration lower than 75 deg/s^2, the sensitivity [0.2 K/(deg/s^2)] and response speed (693 μs) are better using a hemispherical chamber than using the conventional rectangular one [0.167 K/(deg/s^2) and 1183 μs].

*Corresponding author: e-mail: jmlin@chu.edu.tw

ISSN 0914-4935 © MYU K.K.

1. Introduction

Conventional linear accelerometers, rate gyros, and angular accelerometers are made on silicon,[1–3] some of them use thermal convection technologies, and the chamber is filled with air, CO_2, liquid, or others. As shown in Fig. 1, five novel ideas are proposed in this paper for integrating an active RFID tag with thermal convection angular accelerometers on a flexible substrate; thus, the device is a wireless sensor. The first idea is that the new device has no movable parts, so it is very reliable. The second new idea is that it is fabricated directly on a flexible substrate, such as plastic or polyimide. Since the thermal conductivity of the flexible substrate such as polyimide [0.06–0.0017 W/(cm-K)] is about twenty-fifth of that of silicon [1.48 W/(cm-K)], the new device can save more power by using the flexible substrate. The third new idea is to use inert xenon gas in the chambers for heat conduction instead of the tranditonal CO_2; the latter can cause oxidation effects on the heater and thermal sensors,[1–6] whereas the xenon gas will not. Thus, the heater reliability and life cycle can be improved. The fourth new idea is to further integrate an active RFID tag with an angular accelerometer on the same flexible substrate. Thus, this device becomes a more useful wireless sensor, which can be applied to many fields, such as navigation, mobile phones, hospital monitoring, and games. The heater temperature is 127 °C without melting the polyimide substrate.

It was reported[7] that the sensitivity of an inclinometer[8] can be increased by using a nonfloating structure on a flexible substrate without a grooved cavity, as in the conventional silicon-based device.[9] Moreover, the chamber was filled with an inert gas such as xenon to avoid the oxidizing effect produced by the previous ones such as carbon dioxide or air.[10–12] Thus, not only the heater reliability but also the device reliability and life cycle could be improved. Besides, the inner shape of the chamber is hemispherical, which could make the sensitivity better than that of the traditional rectangular one.[13] On the other hand, the outer shape of the package can still be rectangular for easy marking of the part name and series number.

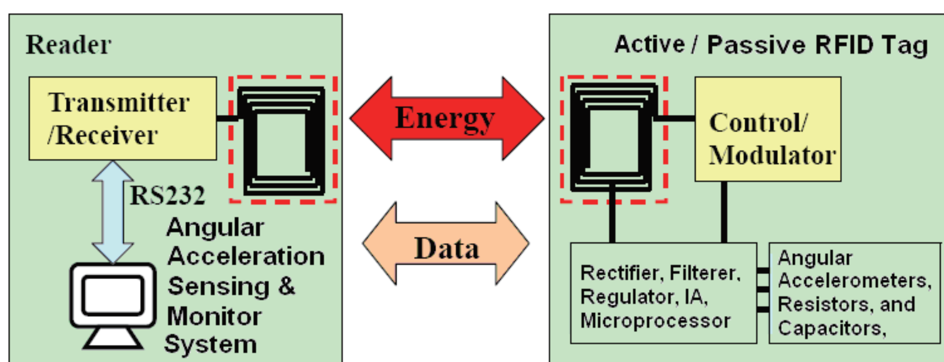

Fig. 1. (Color online) Block diagram of the new RFID-based angular accelerometer.

Thus, in this paper, we extend the previous ideas to fabricate a thermal convection angular accelerometer directly on a flexible substrate without any movable parts.(14–17) Although both the sensitivity and response speed are lower than those of the floating one, the nonfloating-type angular accelerometer may be a choice if reliability and cost are the major concerns. Moreover, for angular acceleration limited below 75 deg/s^2, the sensitivity [0.2 K/(deg/s^2)] and response speed (693 μs) using a hemispherical chamber would be larger than using the conventional rectangular one [0.167 K/(deg/s^2) and 1183 μs]. This paper is organized as follows: § 1 is the introduction; § 2 describes the fabrication and packaging steps; § 3 is simulation and discussion; § 4 is conclusion.

2. Fabrication and Packaging Steps

The fabrication and packaging steps are as follows:

Step 1: Evaporate SiO_2 on both sides of the substrate for thermal, electrical, and humidity isolation. Next, cover a photoresist (PR) on both sides to protect the SiO_2 layers.

Step 2: Evaporate p-type amorphous silicon (green color) of 100–250 μm thickness and use an Nd-YAG laser to anneal it as a polysilicon thermister. Next, cover a layer of PR (gray color) on the front side. Using mask #1 and photolithography and etching processes (PAEPs), allow the PR to remain on the thermister to protect the underlying layer of polysilicon. Next, use KOH solution or RIE to remove polysilicon without PR protection. Figure 2 shows the result.

Step 3: Remove the PR. Evaporate Cr and Ni to be used as heater, RFID antenna, and conductors connected to the power supply. Next, use mask #2 and PAEP to retain the protecting PR on the heater, RFID antenna, and the conductors connected to the power supply. Use sulfuric acid solution to remove the layers of Cr and Ni without PR protection. Remove the PR; the result is shown in Fig. 3.

Step 4: Use mask #3 and PAEP to reserve the PR on the heater, and then flash a layer of gold on the Ni layer by electroless plating. Thus, the conductivities of the RFID antenna and the conductors connected to the power supply would be very good. Besides, the soldering performance on the pads for packaging would be increased.

Step 5: Screen print a plastic or polymer material around the accelerometer as a dam bar, then put a cap with a hemispherical or a traditional rectangular chamber on the dam bar for curing; before sealing it, fill it with carbon dioxide or xenon gas. Finally,

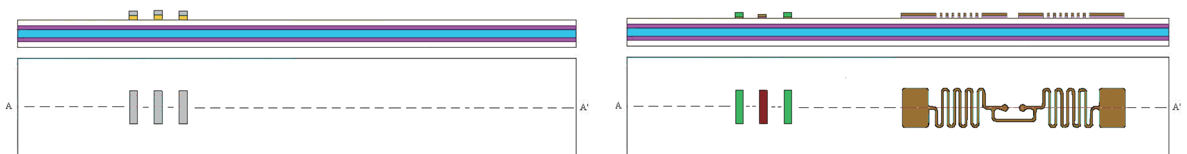

Fig. 2 (left). (Color online) Result of Step 2.
Fig. 3 (right). (Color online) Result of Step 3.

flip-chip-bond the chip with metal bumps to the RFID feed terminals by the thermal compression method, then make the underfill to enhance the chip adherence. The results are as shown in Figs. 4(a) and 5(b).

Step 6: To increase the sensitivity and reduce the drift and bias effects caused by fabrication errors, put four thermisters in a full differential Wheatstone bridge structure. Put a socket and a spring to fix the battery on the substrate.[18–22] Figure 5 shows the top view of the final result.

3. Simulation and Discussion

The ESI-CFD+ software package was used for the simulation and design. For comparison, floating-type angular accelerometers with hemispherical and rectangular chambers as shown respectively in Figs. 6(a) and 6(b) are firstly considered, in which H = 18.7 mm, $W1$ = 2 mm, S = 3 mm, and $W2$ = 0.3 mm, and the floating height of the components, X, is 1 mm. The temperatures of the boundaries and the heaters are set to 300 and 400 K, respectively. The thermal sensors are put at any one of the three points, as shown in Figs. 6(a) and 6(b), for trade-off later.[23–30]

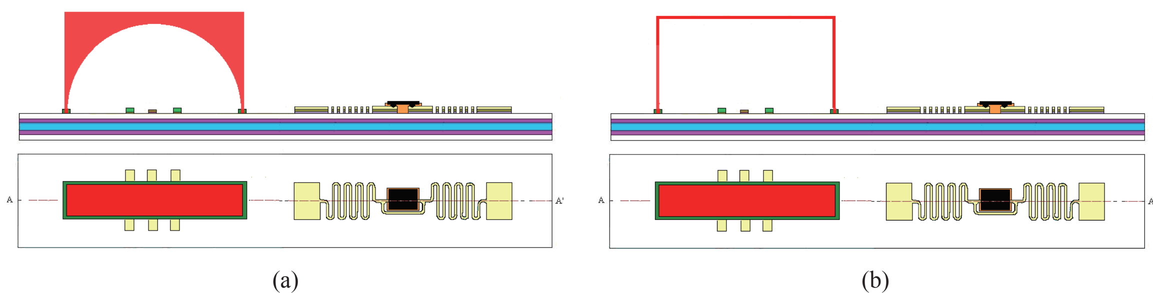

(a) (b)

Fig. 4. (Color online) Results of nonfloating-type angular accelerometers. (a) Hemispherical chamber. (b) Rectangular chamber.

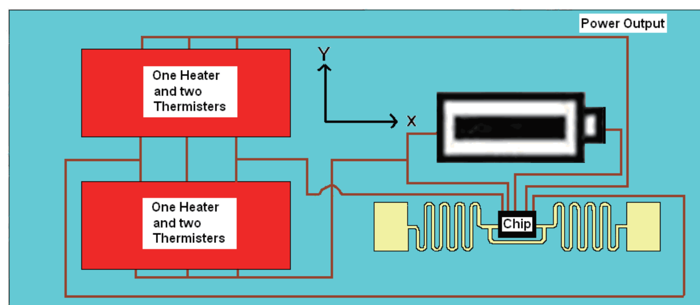

Fig. 5. (Color online) Top view of the final result after Step 6.

3.1 *Results of floating-type angular accelerometer*

The sensitivity curves by using rectangular and hemispherical chambers are as shown in Figs. 7(a) and 7(b), respectively. Note that the sensitivity performances are better using the rectangular chamber than using the hemispherical one, as also listed in Table 1; thus, the thermal sensors located at point 2 (middle) are a good choice.

The temperature distributions on the horizontal plane by using rectangular and hemispherical chambers for angular accelerations of 60, 120, and 180 deg/s^2 are as shown in Figs. 8 and 9, respectively. Note that the temperature differences of thermal

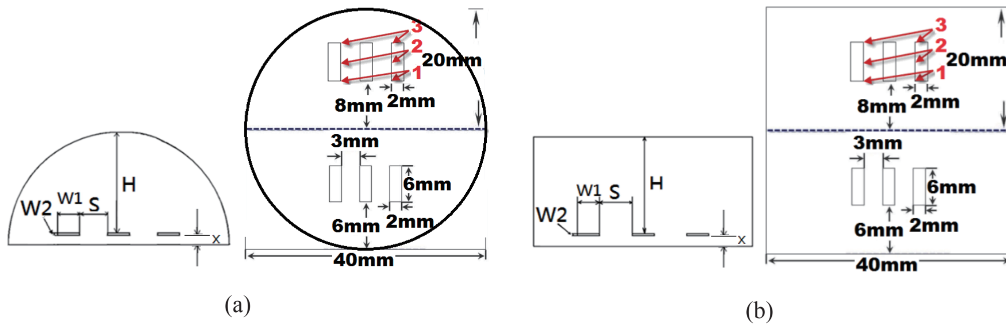

Fig. 6. (Color online) Side and top views of floating-type angular accelerometers. (a) Hemispherical chamber. (b) Rectangular chamber.

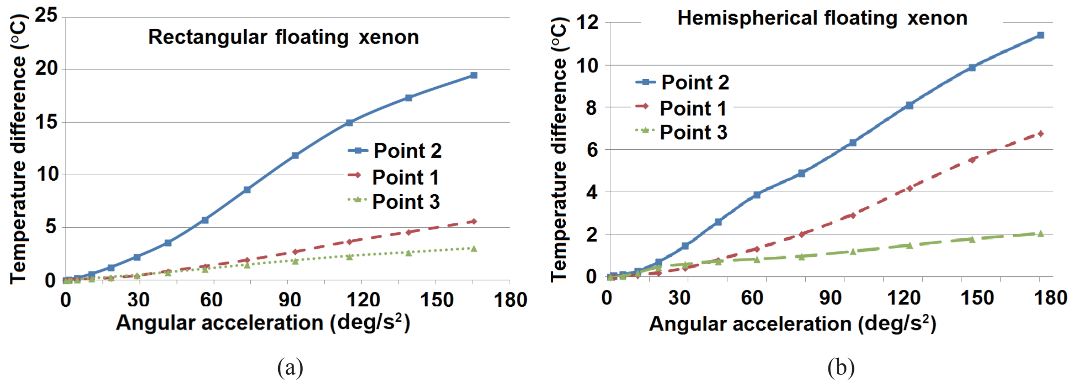

Fig. 7. (Color online) Sensitivity curves of floating-type devices with various chambers. (a) Rectangular chamber. (b) Hemispherical chamber.

Table 1
Sensitivity performance comparison of floating-type devices with various chambers for thermal sensors located at point 2.

Type of chamber	Rectangular	Hemispherical
Sensitivity [K/(deg/s^2)]	0.6945	0.3994

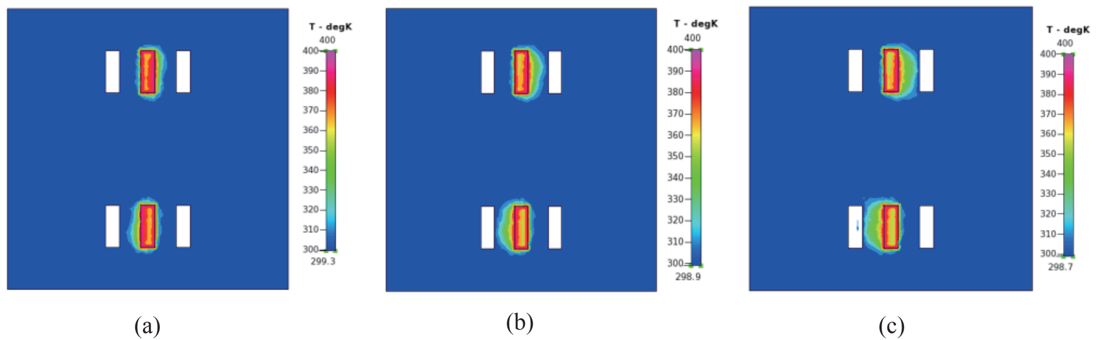

Fig. 8. (Color online) Temperature distributions of floating-type devices on horizontal plane with rectangular chamber for angular accelerations of (a) 60, (b) 120, and (c) 180 deg/s^2.

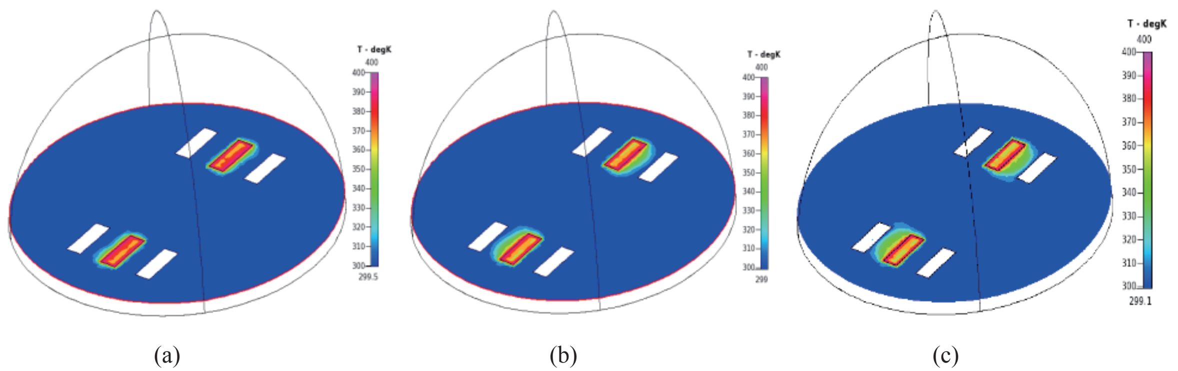

Fig. 9. (Color online) Temperature distributions of floating type devices with hemispherical chamber for angular accelerations of (a) 60, (b) 120, and (c) 180 deg/s^2.

sensors located at point 2 in Figs. 8 and 9 are larger than those at the other points, which coincide with the results shown in Figs. 7(a) and 7(b), respectively. The step-input responses (180 deg/s^2) of the gas total enthalpy (static pressure) and the velocity for the thermal sensors placed at point 2 by using rectangular and hemispherical chambers are as shown in Figs. 10 and 11, respectively.

Moreover, the rise times of gas total enthalpy, static pressure, and velocity for various chambers are listed in Table 2. The average values of the above three responses are also listed in Table 2 for comparison. Note that the sensitivity is better (lower) using the rectangular (hemispherical) chamber as mentioned previously, but the response speed is slower (faster). Thus, one can choose either one depending on which requirement is preferred.

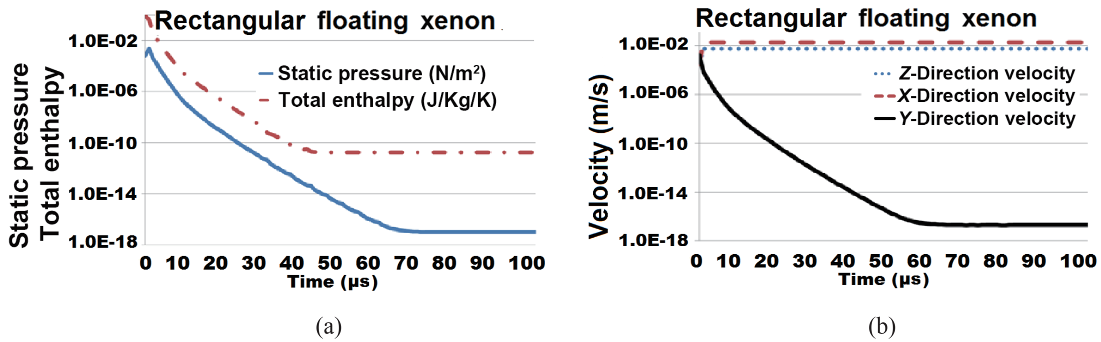

Fig. 10. (Color online) Step-input responses of (a) gas total enthalpy, static pressure, and (b) velocity for floating-type devices with rectangular chamber.

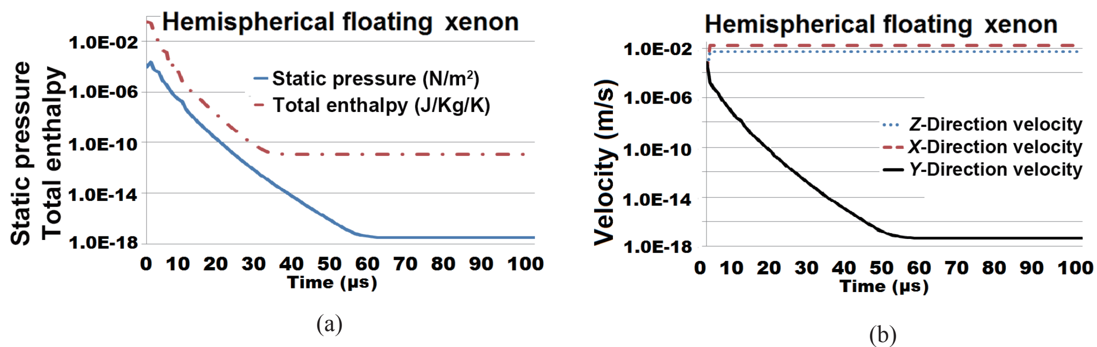

Fig. 11. (Color online) Step-input responses of (a) gas total enthalpy, static pressure, and (b) velocity for floating-type devices with hemispherical chamber.

Table 2
Rise times comparison for step-input responses of floating-type angular accelerometers using various chambers.

Type of chamber	Total enthalpy (μs)	Static pressure (μs)	Velocity (μs)	Average response times of total enthalpy, static pressure, and velocity (μs)
Rectangular	470	700	610	593
Hemispherical	400	600	530	510

3.2 *Nonfloating-type angular accelerometer*

The sensitivity curves by using rectangular and hemispherical chambers are as shown in Figs. 12(a) and 12(b), respectively. On the other hand, the temperature distributions on the horizontal plane of nonfloating-type devices by using xenon gas to fill the rectangular and hemispherical chambers for several angular accelerations (such as

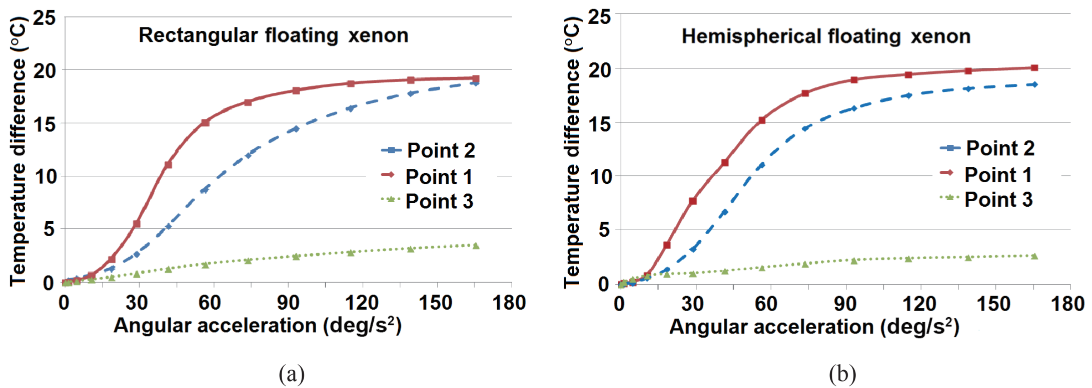

Fig. 12. (Color online) Sensitivity curves of nonfloating-type devices by using (a) rectangular and (b) hemispherical chambers.

60, 120, and 180 deg/s^2) are as shown in Figs. 13 and 14, respectively. Note that the performances of linearity and sensitivity using the rectangular chamber and putting the thermal sensors at point 2 are still better; the sensitivity for the angular acceleration of less than 75 deg/s^2 is also listed in Table 3 for comparison. Figures 13 and 14 show the reasons for the nonlinear effects shown in Figs. 12(a) and 12(b) with the nonfloating structure and putting the thermal sensors at points 1 and 2. Since the thermal sensors are too close to the heaters, the interactions of the gas and the thermal sensors would be more serious at angular accelerations larger than 60 deg/s^2, and then the sensitivity of the devices would be saturated by placing the sensors at points 1 and 2, as shown in Figs. 12(a) and 12(b). However, the interactions of the gas and thermal sensors at point 3 are lower, so the device sensitivities at point 3 are more linear, as shown in Figs. 12(a) and 12(b), but the sensitivities of which are very small for both cases.

The step-input responses (180 deg/s^2) of the gas total enthalpy, static pressure, and velocity for the thermal sensors by using rectangular and hemispherical chambers are as shown in Figs. 15 and 16, respectively. Moreover, the rise times of gas total enthalpy, static pressure, and velocity for various chambers are also listed in Table 4. The average values of the above three responses are also listed in Table 4 for comparison. Note that the response speed is also faster (slower) by using a hemispherical (rectangular) chamber, but they are still slower than those of floating-type devices.

3.3 *Discussion*

From the above simulations, one can see by using either a rectangular or hemispherical chamber, that not only the response speeds but also the sensitivities of the floating-type angular accelerometer are better than those of the nonfloating ones. The advantage of using the hemispherical ones is that they are always faster than the rectangular ones for both types. However, the nonfloating-type angular accelerometer may be a choice if reliability and cost are the major concerns. Moreover, for angular

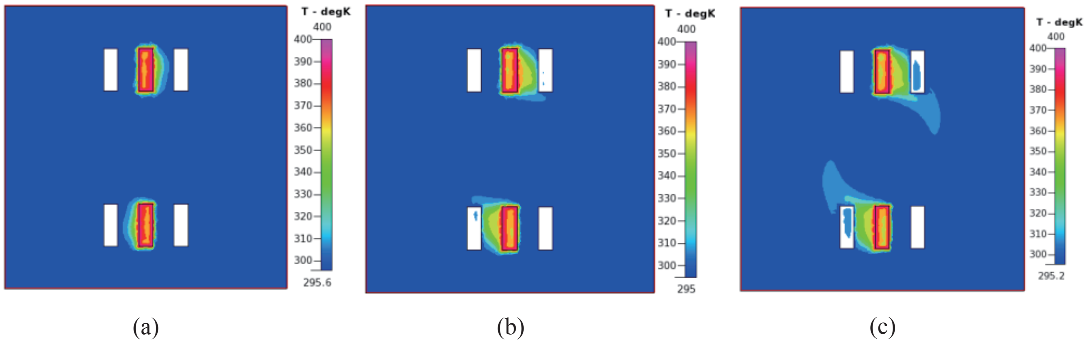

(a) (b) (c)

Fig. 13. (Color online) Temperature distributions of nonfloating-type devices on horizontal plane with rectangular chamber for angular accelerations of (a) 60, (b) 120, and (c) 180 deg/s^2.

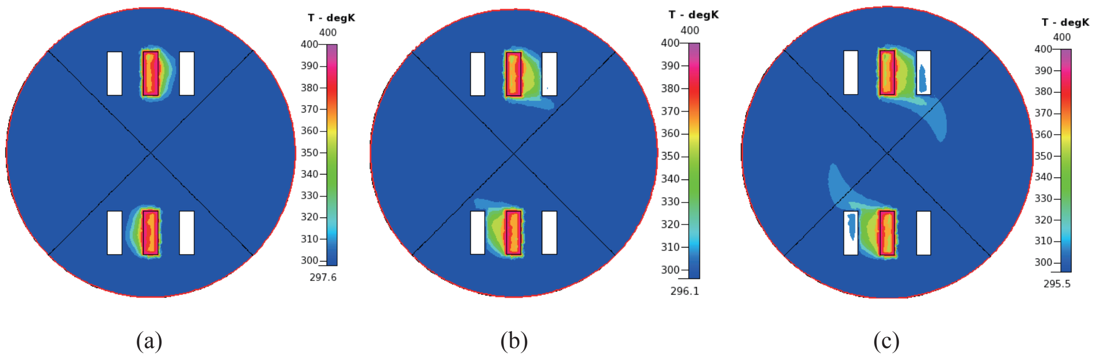

(a) (b) (c)

Fig. 14. (Color online) Temperature distributions of nonfloating-type devices on the horizontal plane with hemispherical chamber for angular accelerations of (a) 60, (b) 120, and (c) 180 deg/s^2.

Table 3
Sensitivity performance comparison of nonfloating-type devices with various chambers for thermal sensors located at point 2.

Type of chamber	Rectangular	Hemispherical
Sensitivity [K/(deg/s^2)] (for angular acceleration less than 75 deg/s^2)	0.167	0.2

acceleration limited below 75 deg/s^2, the sensitivity [0.2 K/(deg/s^2)] and the response speed (693 μs) are better using a hemispherical chamber than using the conventional rectangular one (0.167 K/deg/s^2 and 1183 μs).

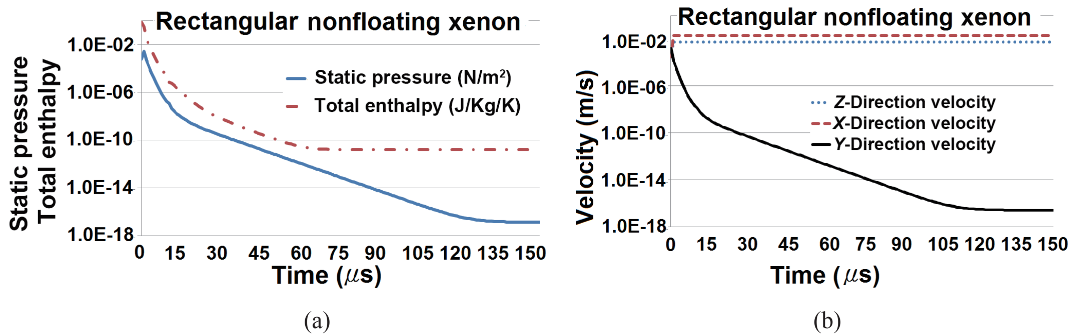

Fig. 15. (Color online) Step-input responses of (a) total enthalpy, static pressure, and (b) velocity for nonfloating-type devices with rectangular chamber.

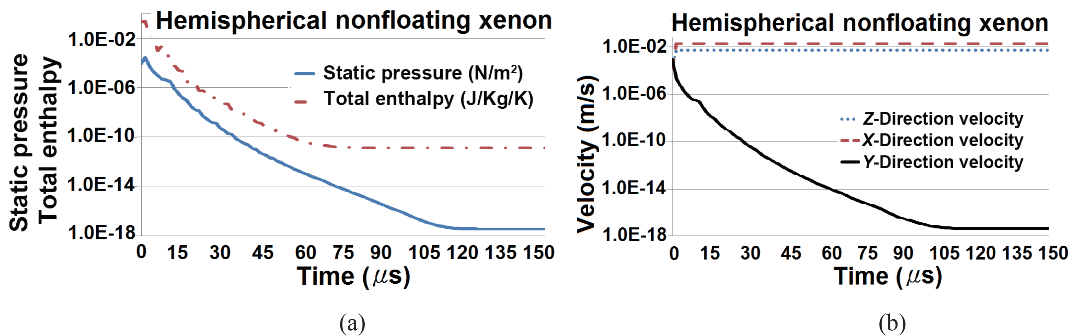

Fig. 16. (Color online) Step-input responses of (a) total enthalpy, static pressure, and (b) velocity for nonfloating-type devices with hemispherical chamber.

Table 4
Rise times comparison for step-input responses (180 deg/s²) of nonfloating-type angular accelerometers using various chambers.

Type of chamber	Total enthalpy (μs)	Static pressure (μs)	Velocity (μs)	Average response times of total enthalpy, static pressure, and velocity (μs)
Rectangular	770	1500	1280	1183
Hemispherical	520	810	750	693

4. Conclusions

Five novel ideas are proposed in this paper to integrate an active RFID tag with a thermal convection angular accelerometer on a flexible substrate. The first innovative idea is that this device is directly made on a flexible substrate. The second new idea is that it is made on a plastic substrate. The third new idea is to apply xenon gas in the

chamber. The fourth new idea is to further integrate an angular accelerometer with an active RFID tag on the same substrate. The final new idea is to apply a hemispherical chamber instead of the conventional rectangular one. The performances (such as reliability, power consumption, wireless ability, and life cycle) of the new device are better. The results show that the nonfloating-type angular accelerometer may be a choice if reliability and cost are the major concerns. Moreover, for angular acceleration limited below 75 deg/s^2, the sensitivity [0.2 K/(deg/s^2)] and the response speed (693 μs) are better using a hemispherical chamber than using the traditional rectangular one [0.167 K/(deg/s^2) and 1183 μs].

Acknowledgements

We thank the National Science Council for Grant Nos. NSC 101-2622-E-216-001-CC3, 101-2221-E-216-006-MY2, 101-2221-E-216-019-, and 102-2622-E-216-002-CC2, and the Ministry of Science and Technology for Grant No. MOST 103-2221-E-216-022. We also thank the National Center of High-Performance Computing (NCHC) for computer time and facilities, including the ESI-CFD+ software package.

References

1 B. Alain, R. Alain, V. Bernard and G. Alain: European Patent No. 1550874 (2010).
2 G. Piazza and P. Stephanou: Micromechanical Thermo-Fluidic Single-Axis Yaw Rate Sensor (University of California, Berkeley, 2002).
3 J. Bahari and A. M. Leung: J. Micromech. Microeng. **21** (2011) 1.
4 J. Courteaud, N. Crespy, P. Combette, B. Sorli and A. Giani: Sens. Actuators, A **147** (2008) 75.
5 J. Dido, P. Loisel and A. Renault: U.S. Patent No. 7426862 B2 (2008).
6 F. Peluso, D. Castagnolo and C. Albanese: Microgravity Sci. Technol. **13** (2002) 41.
7 J. M. Lin and C. H. Lin: Proceedings of 2013 International Conference on Computer, Networks and Communication Engineering (Beijing, 2013) pp. 569–572.
8 F. Khoshnoud and C. W. de Silva: IEEE Instrum. Meas. Mag. **15** (2012) 14.
9 A. Garraud, A. Giani, P. Combette, B. Charlot and M. Richard: Sens. Actuators, A **170** (2011) 44.
10 Y. Zhao, A. P. Brokaw, M. E. Rebeschini, A. M. Leung, G. P. Pucci and A. Dribinsky: U.S. Patent No. 6795752 B1 (2004).
11 Y. Zhao, A. Leung, M. E. Rebeschini, G. P. Pucci, A. Dribinsky and Y. Cai: U.S. Patent No. 7305881 B2 (2007).
12 A. Dribinsky, G. P. Pucci, Y. Cai, M. O'Brien, G. J. Varghese, Y. Zhao and Y. Y. Cai: U.S. Patent No. 7862229 (2011).
13 T. R. Hsu: MEMS & Microsystems (McGraw-Hill Companies Inc., Boston, 2002).
14 K. M. Liao, R. Chen and B. C. S. Chou: Sens. Actuators, A **130–131** (2006) 282.
15 L. Lin, R. T. Howe and A. P. Pisano: IEEE J. Microelectromech. Syst. **7** (1998) 286.
16 L. C. Spangler and C. J. Kemp: Sens. Actuators, A **54** (1996) 523.
17 A. Petropoulosa, A. Moschosa, S. Athineosa and G. Kaltsas: Procedia Eng. **25** (2011) 643.
18 R. Dao, D. E. Morgan, H. H. Kries and D. M. Bachelder: U.S. Patent No. 5581034 (1996).
19 A. A. Rekik, F. Azaïs, N. Dumas, F. Mailly and P. Nouet: J. Electron. Test. **27** (2011) 41.
20 T. Mineta, S. Kobayashi, Y. Watanabe, S. Kanauchi, I. Nakagawa, E. Suganuma and M. Esashi: J. Micromech. Microeng. **6** (2001) 431.

21 U. A. Dauderstadt, P. H. S. de Vries, R. Hiratsuka, J. G. Korvink, P. M. Sarro, H. Baltes and S. Middelhoek: Sens. Actuators, A **55** (1996) 3.
22 U. A. Dauderstadt, P. M. Sarro and P. J. French: Solid State Sens. Actuators **66** (2008) 244.
23 B. Luo, Z. X. Li, Z. Y. Guo and Y. J. Yang: J. Micromech. Microeng. **11** (2001) 504.
24 A. H. Ma and A. M. Leung: Proc. IEEE Sens. (2008) 1492.
25 G. Daia, M. Li, X. P. He, L. M. Du, B. B. Shao and W. Su: Sens. Actuators, A **172** (2011) 369.
26 L. A. Rocha, C. S. Silva, M. F. Cerqueira, J. F. Ribeiro, L. M. Goncalves, A. J. Pontes and J. C. Viana: Procedia Eng. **25** (2011) 607.
27 Y. Hua, Z. Li and H. Xaio: U.S. Patent No. 8011226 B2 (2011).
28 R. Zhu, H. Ding, Y. Su and Y. Yang: Sensors **10** (2010) 8304.
29 T. Dau, D. V. Dao, T. Shiozawa, H. Kumagai and S. Sugiyama: J. Micromech. Microeng. **16** (2006) 1301.
30 A. Ya'akobovitz and S. Krylov: IEEE J. Sens. **10** (2010) 1311.